Progress In Electromagnetics Research B, Vol. 62, 87–103, 2015

Novel Wearable Eagle Shape Microstrip Antenna Array with Mutual Coupling Reduction

Mohamed I. Ahmed[1, *], Esmat A. Abdallah[1], and Hadia M. Elhennawy[2]

Abstract—Novel eagle shape microstrip wearable antennas (element and array) are presented. The single- and two-element antenna arrays are designed and fabricated on a Roger RT/Duroid 5880 substrate with dielectric constant of 2.2, thickness of 1.5748 mm, and $\tan\delta = 0.001$. The measured results show that a reduction in mutual coupling of 36 dB is achieved at the first band (1.68–2.65) GHz and 22.1 dB over the second band (6.5–8.86) GHz due to introducing electromagnetic bandgap (EBG) structures. EBG structure has an eagle-like shape with more gaps. By increasing the number of EBG cells and varying the gap distance between cells to certain limit, the mutual coupling reduction is improved. Also, a size reduction of 80% is achieved. The microstrip array was simulated by CST simulator version 2014 and fabricated by proto laser machine with precision 25 µm. The specific absorption rate (SAR) investigation is carried out on CST2014 Simulator. Maximum SAR value is 1.953 W/kg which indicates that the eagle-shaped microstrip wearable antennas are safe for human. The antennas can be used in the official or RFID applications.

1. INTRODUCTION

One of the dominant research topics in antennas for body-centric communications is wearable and fabric-based antennas. Commonly, wearable antennas for all modern applications require light weight, low cost, almost maintenance-free and no installation. There is a number of specialized occupation segments that utilize body centric communication systems, such as paramedics, fire fighters, and military. Besides, wearable antennas can also be applied to youngsters, the aged, and athletes for the purpose of monitoring [1].

The electromagnetic absorption of a human body has become an important issue, as governments strictly limit it. Due to the extensive spread of wearable antenna, the radiation of wearable antenna has rapidly been given increased attention. The radiation can be evaluated by specific absorption rate (SAR), which represents the time rate of microwave energy absorption inside the tissue, as follows:

$$\mathrm{SAR} = \frac{\sigma}{2\rho}|E|^2 \tag{1}$$

where ρ and σ are the density (kg/m^3) and electrical conductivity (S/m) of the tissue, respectively, and E is the internal induce electrical field (V/m). The SAR value is calculated as the maximum of mass-averaged SAR and is strictly limited by governments. Nowadays, two standards of SAR are adopted: Europe uses 2 W/kg averaged over 10 g tissue (over 10 g tissue means to average the SAR values in a volume with an average mass of 10 g) [2]. Meanwhile, the U.S. Federal Communication Commission (FCC) requires that the SAR should be lower than 1.6 W/kg averaged over 1 g tissues. Due to the lower limited value and smaller averaged mass, the standard from FCC (1.6 W/kg) is more difficult to satisfy than the one from EU (2 W/kg) with average time of 6 minutes [3].

Received 9 December 2014, Accepted 5 February 2015, Scheduled 16 February 2015
* Corresponding author: Mohamed Ismail Ahmed (miahmed@eri.sci.eg).
[1] Electronics Research Institute, Cairo, Egypt. [2] Ain Shams University, Cairo, Egypt.

Rapid growth of wireless technologies in recent years has made the antennas designs more challenging. Antenna arrays can significantly improve the efficiency of wireless application systems. Antennas can satisfy applications, such as digital communication, GPS, GSM, WLAN and RFID. For above mentioned applications antenna array devices with resonant frequency of 2.4 to 2.485 GHz are used. However, patch antenna arrays have several major drawbacks, such as: 1) Mutual coupling loss, 2) Size of antenna, and 3) Narrow bandwidth [4]. Mutual coupling in arrays is considered a very import problem; hence it is given much attention from antenna design engineers. By placing EBG cells in between the patch antennas, mutual coupling can be reduced significantly [5]. An EBG structure has the ability of suppressing the surface wave propagation in significant frequency band, known as band gap feature. The features of EBGs are extended to improve array antenna performance by increasing the directivity such as increasing antenna gain and reducing back radiation. To increase the capacitance effect of the equivalent LC circuit and to improve the compactness in EBG structures, different shapes with significant gaps are investigated [6]. The practical applications of EBG structures have difficulties in accommodating their physical sizes [7, 8]. Another major drawback of patch antennas array is narrow bandwidth. A possible way to increase the bandwidth is to either increase the height of the dielectric or decrease the dielectric constant.

In this paper, the first two drawbacks are analyzed, and the simulated and measured results are obtained. This configuration is chosen because the eagle shape is the official badge for most of Middle East official applications. So, this antenna may be used in soldier berets or belts, and any commodity for the official applications. It should be noted that its main application depends on the range of frequency. According to the chosen ranges of the operating frequency it can be used in RFID or in communication systems. A novel eagle-shaped wearable microstrip antenna array with EBG cells is applied to reduce the mutual coupling between array elements with the same shape. The results show that a reduction in mutual coupling of 36 dB is achieved at the first band (1.68–2.65) GHz and 22.1 dB at the second band (6.5–8.86) GHz. The paper is organized as follows. Section 2 introduces the antenna design and simulation. Section 3 gives the experimental results and discussion. SAR calculation is introduced in Section 4, while conclusion is introduced in Section 5.

2. ANTENNA DESIGN AND SIMULATION

This section is divided into three parts. The first part discusses the single element geometry of the novel eagle-shaped microstrip patch antenna. The second part presents the two elements of the novel eagle-shaped microstrip patch array arranged on a substrate without EBG and studies the effect of spacing between elements on the mutual coupling. The last part of this section shows the two elements of the novel eagle-shaped microstrip patch antenna array arranged on the substrate with EBG elements having the same shape as array patches (eagle shape). The E- and H-plane radiation patterns are discussed in each antenna model. Each antenna structure is modeled in CST Design Suite 2014 Microwave Studio in which extensive full-wave analysis is performed based on integral equation method.

2.1. Single Element

CST numerical simulator is used to simulate the eagle-shaped microstrip patch antenna etched on a dielectric substrate Roger RT/Duroid 5880 with $\varepsilon_r = 2.2$, $h = 1.5748$ mm, and $\tan\delta = 0.001$ which is similar to the Egyptian army beret eagle. The design process starts with printed monopole rectangular patch microstrip antenna. Then, the rectangular shape is changed through four steps to reach the acceptable shape of real eagle at the resonant frequency of 2.4 GHz as shown in Fig. 1(a). The patch's size $W_p \times L_p$ is 17 mm × 23 mm. This dimension represents the minimum dimension of a rectangle that contains the eagle shape inside it. The substrate size $W_{\text{sub}} \times L_{\text{sub}}$ is 30 mm × 50 mm ($0.33\lambda_g \times 0.55\lambda_g$) at resonant frequency to avoid fringing effect where λ_g is the guide wavelength at $f = 2.4$ GHz. Fig. 1(a) shows five design cases: case 1 (conventional patch), case 2 (patch with head), case 3 (patch with head and middle slot), case 4 (patch with head, middle slot, and wings slits), and case 5 (eagle shape patch). The real slogan on Egyptian army beret is shown in Fig. 1(b). The optimum value of the ground plane height is $L_{gp} = 19.7$ mm as shown in Fig. 1(c). The patch is fed by a matched microstrip line fed with width $W_{50} = 4.8$ mm. When comparing the conventional microstrip patch's area 49.4 mm × 41.3 mm

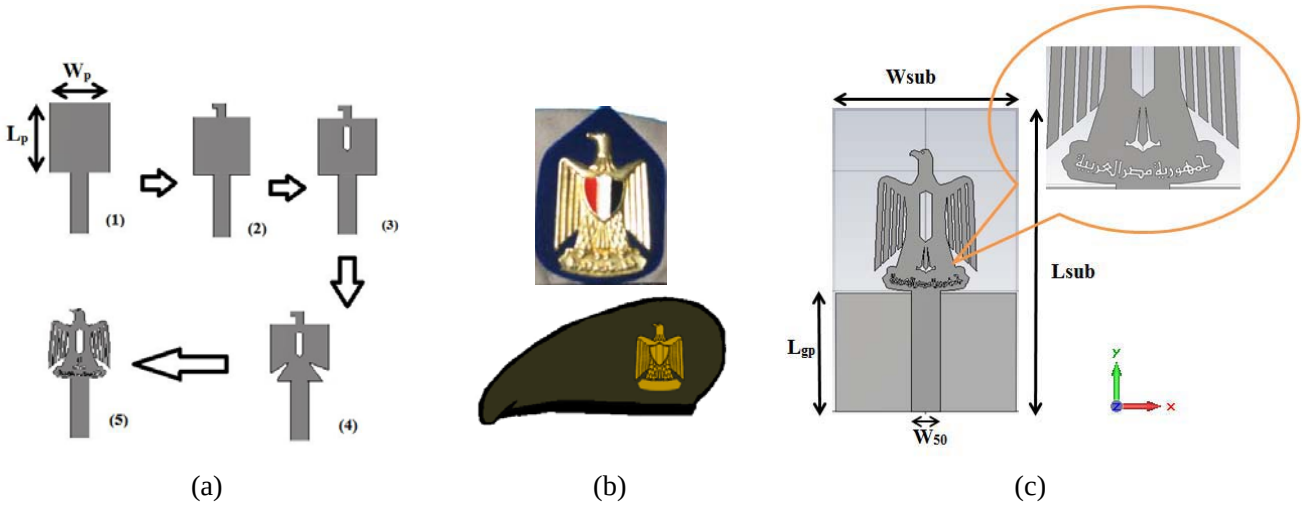

Figure 1. Design steps of the novel eagle shape microstrip patch antenna. (a) The five design cases, (b) the real slogan on Egyptian army beret, and (c) the proposed design.

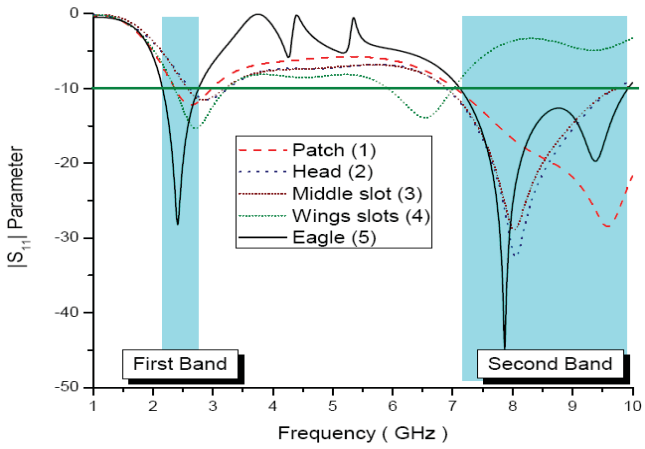

Figure 2. The reflection coefficient $|S_{11}|$ dB comparison among the five cases.

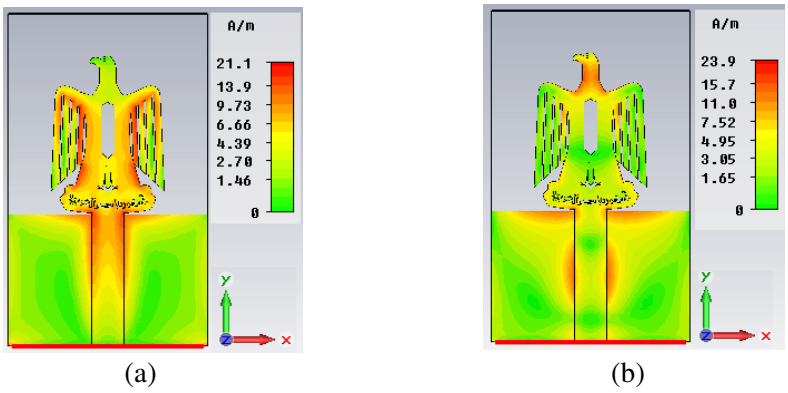

Figure 3. Surface current distribution of novel eagle shape microstrip single element antenna at frequencies. (a) 2.413 GHz, and (b) 7.867 GHz.

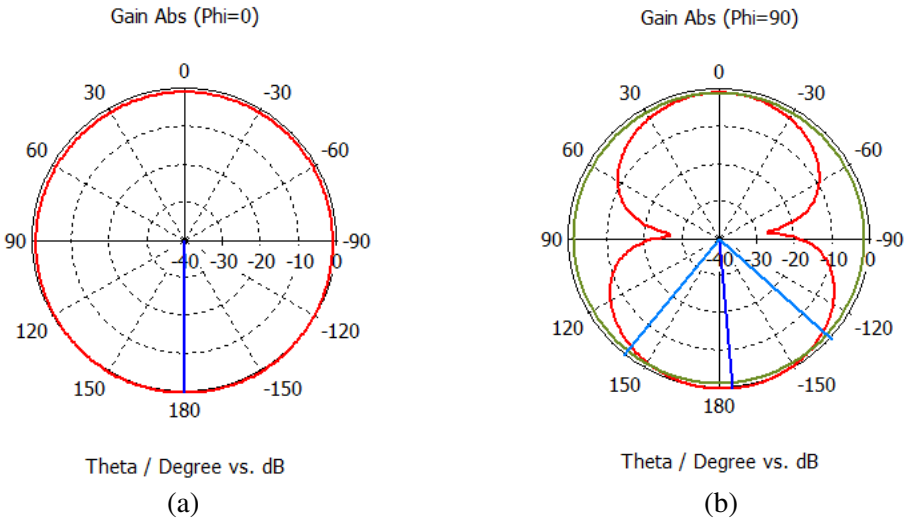

(a) (b)

Figure 4. Radiation pattern of novel eagle shape microstrip single element antenna at frequency 2.413 GHz. (a) E-plane (XZ), and (b) H-plane (YZ).

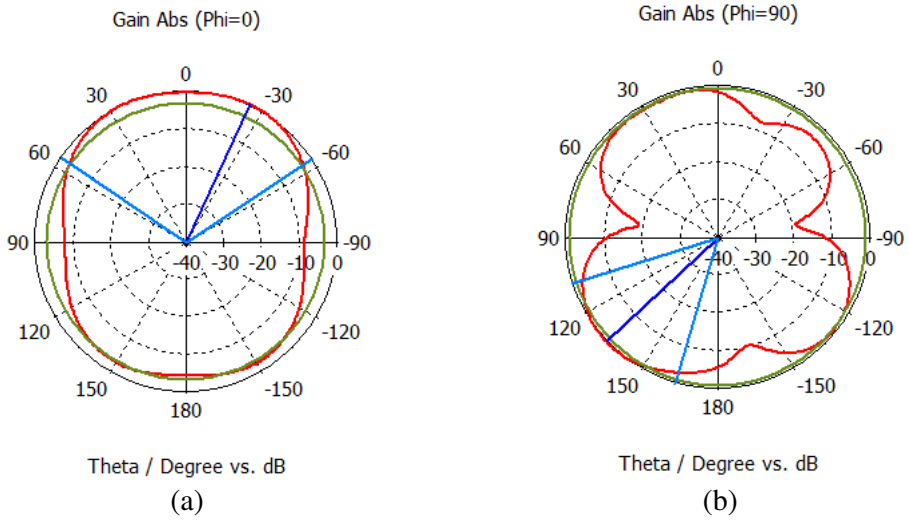

(a) (b)

Figure 5. Radiation pattern of novel eagle shape microstrip single element antenna at frequency 7.867 GHz. (a) E-plane (XZ), and (b) H-plane (YZ).

operating at 2.4 GHz with the proposed one, an area reduction of 80% is obtained [9]. Fig. 2 presents the comparison between the reflection coefficients of the five design cases.

Two bands of frequencies are obtained. The first band (2.164–2.751 GHz) and second band (7.114–9.915 GHz) are based on −10 dB reflection coefficient. Fig. 3(a) shows that the current is concentrated around the middle and wings parts of the eagle shape at resonant frequency 2.413 GHz. At the second resonant frequency 7.867 GHz, the surface current distribution indicates that the current is concentrated around the head of the eagle shape as shown in Fig. 3(b). The omnidirectional radiation patterns at E- and H-planes for both bands of frequency are shown in Fig. 4 and Fig. 5, respectively. In Table 1, single patch antenna parameters are presented. It is observed that the novel antenna achieves wider bandwidth in the second band, good matching, acceptable gain, and good radiation efficiency.

In order to investigate the bending effect of the single element antenna, multiple parametrical studies have been carried out. The simulations prove that there is no noticeable impact on the antenna performance in terms of impedance bandwidth and radiation characteristics. Fig. 6 shows the bending effect on the reflection coefficient $|S_{11}|$ for different curvature radii (from 100 mm to 500 mm).

Table 1. Novel eagle shape microstrip patch antenna.

Parameters	first band (2.164–2.751 GHz)	second band (7.114–9.915 GHz)
Frequency (GHz)	2.413	7.867
$\|S_{11}\|$ (dB)	−28.2	−44.8
F.B.W. %	23	33
Gain (dBi)	2.275	3.151
F/B ratio	1.37	3.59
H.P.B.W (deg.)	-	110.6
Radiation efficiency	89.3%	94%
Antenna efficiency	89.2%	93%

2.2. Two Elements Array without EBG

Figure 7 shows the schematic diagram of the two-element array of the novel eagle-shaped microstrip patch antenna on the same dielectric substrate as single element. The antennas separation distance is chosen to be 40 mm ($\approx 0.3\lambda_0$) after optimization to reduce the mutual coupling, avoid grating lobes, and obtain the omnidirectional (figure of eight radiation pattern) where λ_0 is the free space wavelength at $f = 2.359$ GHz. Parametric study on the element's separation was carried out to obtain the least

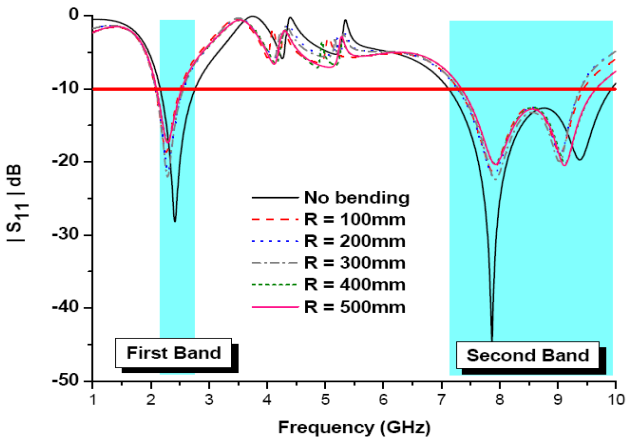

Figure 6. The reflection coefficient $|S_{11}|$ comparison in case of using multiple the curvature radii.

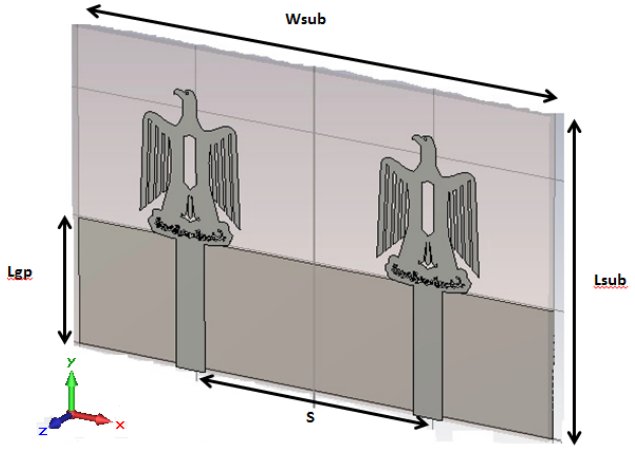

Figure 7. The two elements of novel eagle shape microstrip antenna array.

Table 2. Two elements of novel eagle shape microstrip patch antenna without EBG.

Parameters	first band (2.098–2.727 GHz)	second band (7.01–10 GHz)
Frequency (GHz)	2.359	9.55
$\|S_{11}\|$ (dB)	−36.37	−25.7
$\|S_{21}\|$ (dB)	−12.8	−18.7
F.B.W. %	26.2	31.3
Gain (dBi)	3.1	4.953
F/B ratio	1.32	4.23
H.P.B.W (deg.)	92.8	30.4
Radiation efficiency	95%	93%
Antenna efficiency	90%	91%

separation with optimum coupling. The largest separation 60 mm results in the lowest mutual coupling but the worst in the reflection coefficient as shown in Fig. 8(a). So, we choose 40 mm separation to obtain good matching and suitable mutual coupling as displayed in Fig. 8(b). The ground plane is 80 mm × 50 mm ($2.1\lambda_0 \times 1.3\lambda_0$) at resonant frequency. Each patch is fed by a matched 50 Ω microstrip line feed with width $W_{50} = 4.8$ mm. From Table 2, it is noticed that the mutual coupling in the first and second bands are −12.8 dB and −18.7 dB, respectively. This difference can be accounted to the effect of the distance separation between elements in the two frequency bands compared to the wavelength of each band. The simulated gain and radiation efficiency are presented in Table 2.

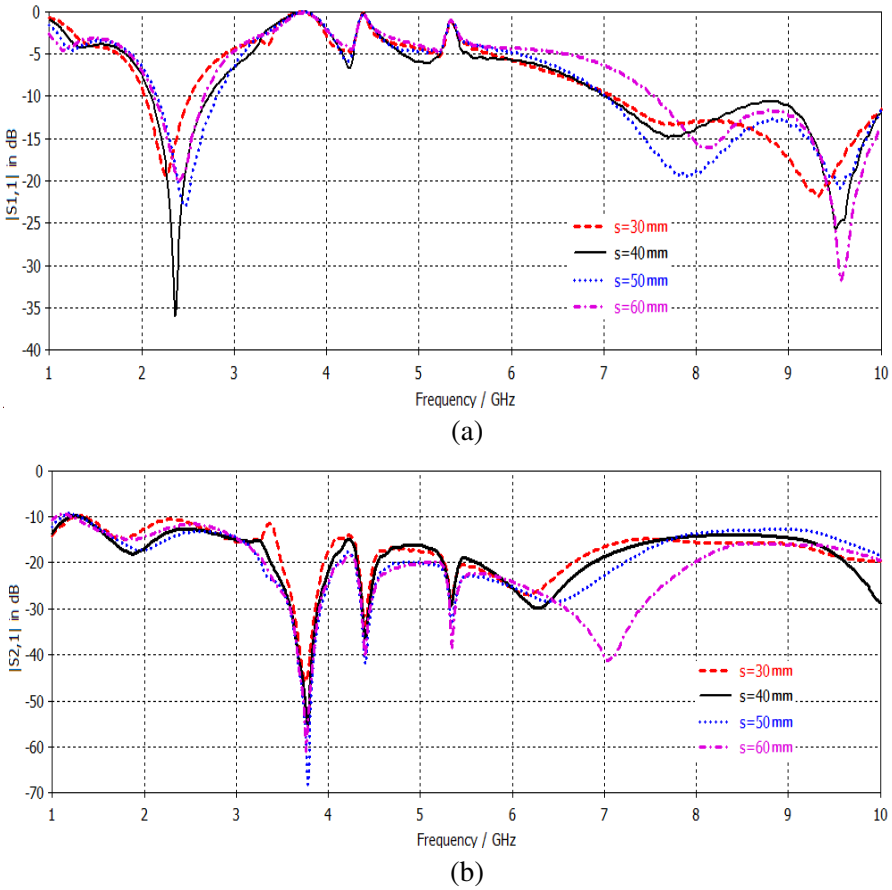

Figure 8. The effect of varying the separation distance between the array elements. (a) $|S_{11}|$, and (b) $|S_{21}|$.

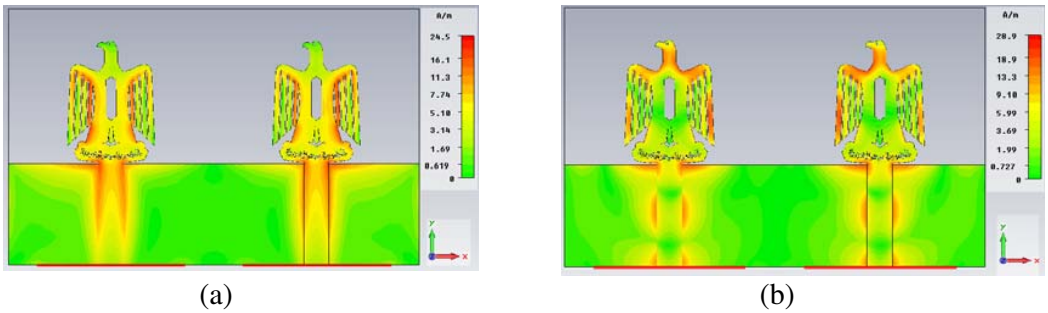

Figure 9. Surface current distributions of novel eagle shape microstrip antenna array without EBG at frequencies. (a) 2.359 GHz, and (b) 9.55 GHz.

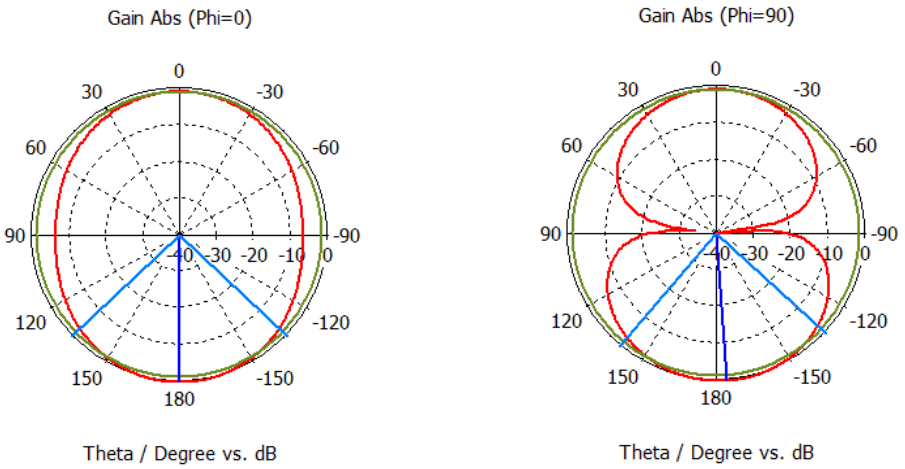

(a) (b)

Figure 10. Radiation pattern of novel eagle shape microstrip antenna array without EBG at frequency 2.359 GHz. (a) E-plane (XZ), and (b) H-plane (YZ).

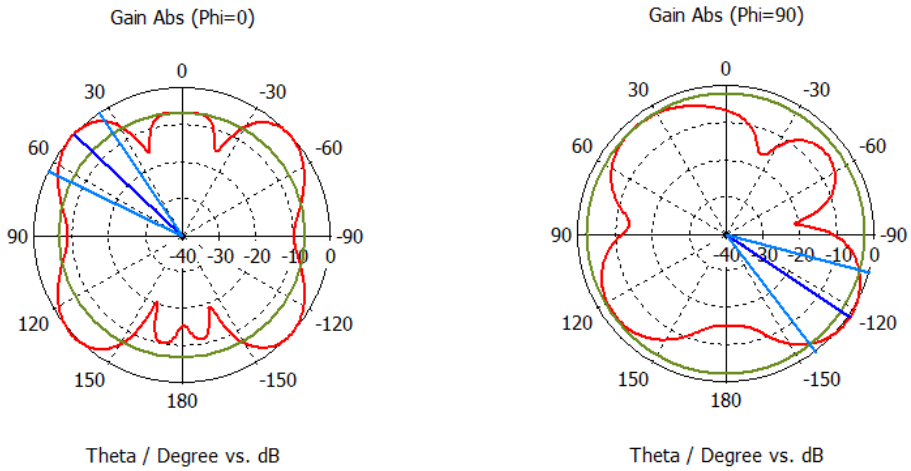

(a) (b)

Figure 11. Radiation pattern of novel eagle shape microstrip antenna array without EBG at frequency 9.55 GHz. (a) E-plane (XZ), and (b) H-plane (YZ).

At the first resonant frequency of 2.359 GHz, the surface current distribution shows high values at the middle and wings parts of the eagle, which result in good radiation characteristic at this frequency as shown in Fig. 9(a). On the other hand, the head and outer parts of the eagle wings are responsible for the radiation at resonant frequency of 9.55 GHz as shown in Fig. 9(b). The E- and H-plane radiation patterns for two elements without EBG are shown in Fig. 10 and Fig. 11, respectively. The 3-dB beamwidth becomes more directive than single patch.

2.3. Two Elements Array with EBG

The two elements of the novel eagle-shaped microstrip patch antenna with the same patch shape EBG cells are shown in Fig. 12. The distance between the patches 40 mm ($\approx 0.3\lambda_0$) is optimized to reduce the mutual coupling and avoid grating lobes where λ_0 is the free space wavelength at $f = 2.161$ GHz. The ground plane is 80 mm $\times$ 50 mm ($2.1\lambda_0 \times 1.3\lambda_0$) at resonant frequency. Each patch is fed by a matched microstrip line feed with width $W_{50} = 4.8$ mm. The comparison between $|S_{11}|$ and $|S_{21}|$ parameters in dB

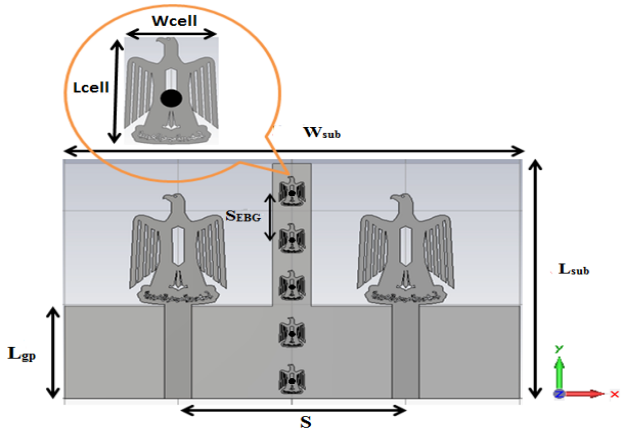

Figure 12. The two element of the novel eagle shape microstrip antenna array with EBG cells.

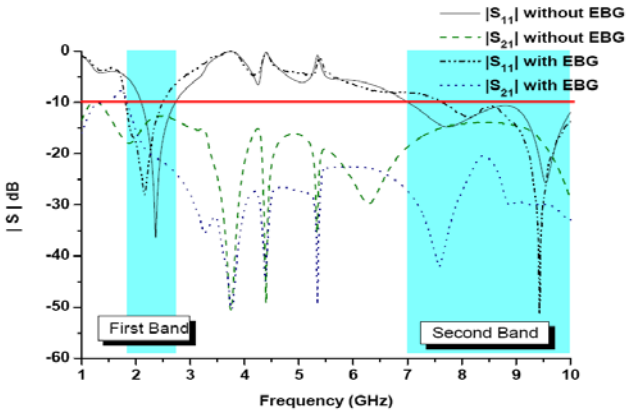

Figure 13. S-parameters of the two elements of the novel eagle shape microstrip antenna array without and with EBG.

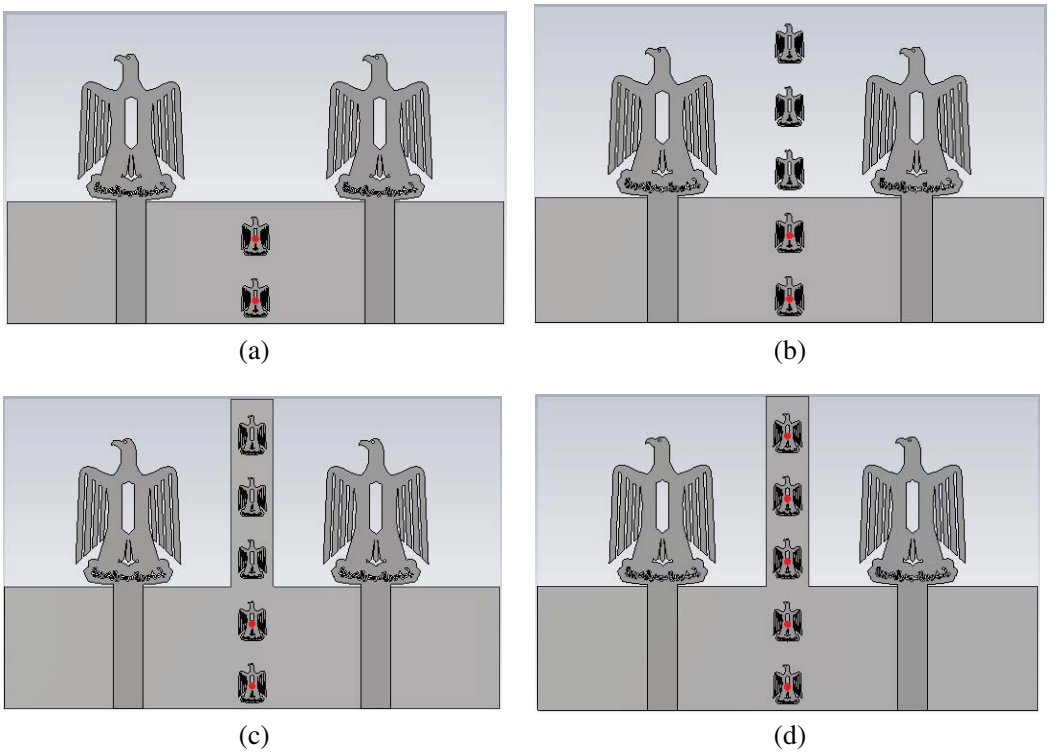

Figure 14. The design steps of the eagle shape EBG cells. (a) Case 1 (only two lower cells with vias), (b) case 2 (adding three upper cells without vias or ground plane strip extension), (c) case 3 (adding three upper cells with ground plane stri), (d) case 4 (adding three upper cells with ground plane strip and vias).

for two elements of the novel eagle-shaped microstrip antenna array without and with EBG is presented in Fig. 13. The mutual coupling difference is 11.7 dB between with and without EBG especially in the second band. The EBG cell size $W_{\text{cell}} \times L_{\text{cell}}$ is 4.5 mm $\times$ 6.3 mm. Both the three upper and two lower EBG cells are connected to the ground plane through vias and separated by $S_{\text{EBG}} = 10$ mm.

The proposed EBG structure has an eagle-like shape which has more gaps. The technique used in this paper, to reduce mutual coupling loss, increases the number of EBG cells and varies the gap distance

between cells. The reduction in mutual coupling by means of periodic structure becomes particularly efficient when grating lobes are avoided. Antenna arrays are mostly large in size, and to improve the performance of the arrays, EBG cells are to be placed in between the patch antennas, which makes the size much larger. So, to reduce the size of the antenna, the proposed method is designing small cells of eagle shape for placing EBG cells with vias closer to the patch antenna placed together in the same

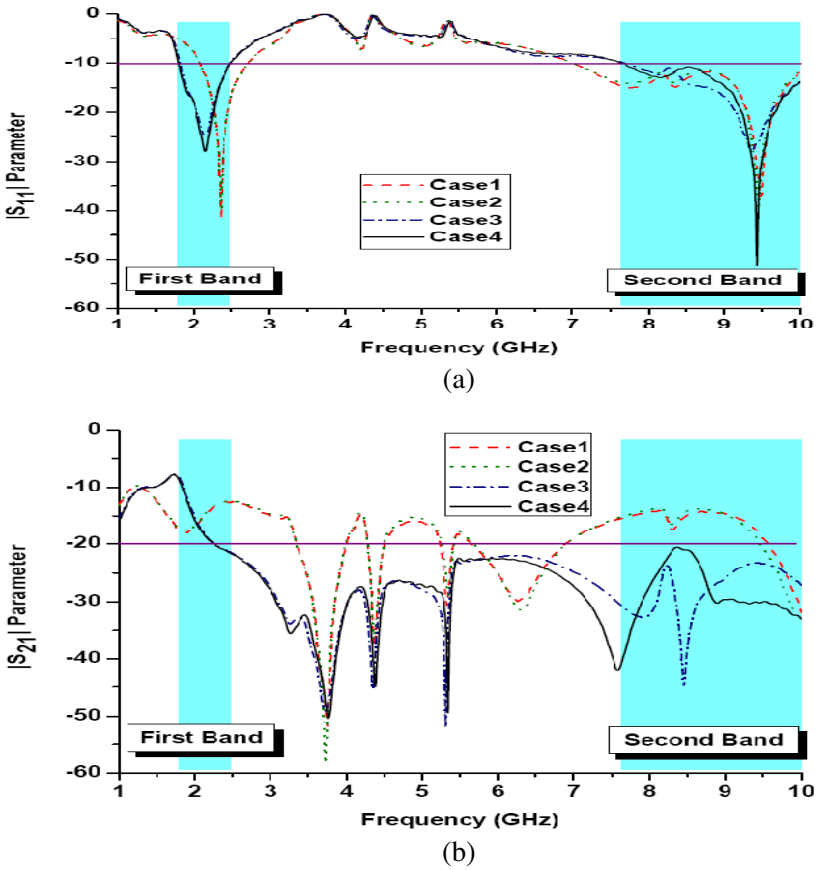

Figure 15. (a) Comparison between simulated $|S_{11}|$ parameters for all cases, and (b) comparison between simulated $|S_{21}|$ parameter for all cases.

Table 3. Two elements of novel eagle shape microstrip patch antenna with EBG.

Parameters	first band (1.81–2.49 GHz)	second band (7.363–10 GHz)
Frequency (GHz)	2.161	9.433
$\|S_{11}\|$ (dB)	−28	−51.3
$\|S_{21}\|$ (dB)	−19	−30.1
B.W. %	31.5	30.4
Gain (dBi)	3.99	6.231
F/B ratio	1.13	8.4
H.P.B.W (deg.)	126	39.7
Radiation efficiency	96%	95%
Antenna efficiency	95%	94%

layer. The design of the proposed EBG cell begins by making down scale by 0.27 from the eagle-shaped patch to get the EBG cell with the same shape as the elements. First, Fig. 14(a) shows only two lower cells connected to the partial ground plane through vias. Second, we increase the number of cells by adding three upper cells with neither vias nor ground plane strip extension as shown in Fig. 14(b). Third, the ground plane strip extension is added under the three upper cells with optimized width of 6.8 mm without any vias connection as displayed in Fig. 14(c). Finally, the last step in EBG design process is shown in Fig. 14(d), where the three upper cells are connected to the ground plane strip extension by means of vias.

The comparison between $|S_{11}|$ parameters in dB for two elements of the eagle-shaped microstrip antenna array with the EBG previous four cases is presented in Fig. 15(a) which proves that the forth case is the best one especially in the second band. Fig. 15(b) shows the comparison between the mutual couplings in dB for the four cases. The acceptable one is the case of five EBG cells with ground plane extension and vias. Table 3 conclude that the mutual coupling in the first and second bands is improved compared to the two elements without EBG. This difference is due to the effect of the EBG cells between elements in the two frequency bands which trap the surface waves and attenuate the surface current as shown in Fig. 16.

At the first resonant frequency 2.161 GHz, the surface current distribution indicates that the middle and wings parts of the eagle shape are responsible for the radiation as shown in Fig. 16(a). The three upper cells reduce undesired surface wave resulting in lower mutual coupling between the array elements. The surface current distribution indicates that the elements have radiation around head and outer parts

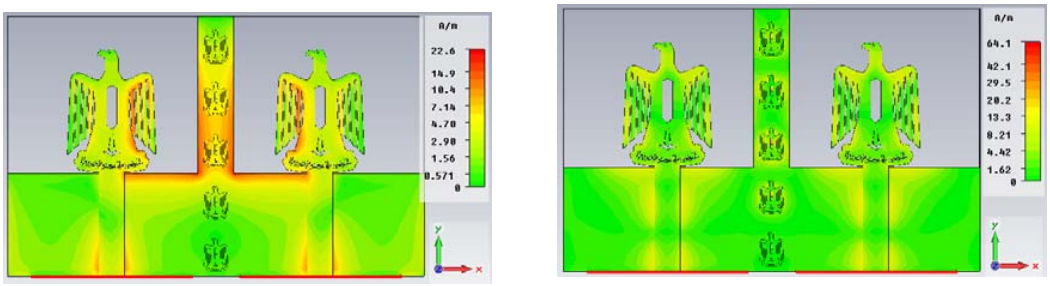

(a) (b)

Figure 16. Surface current distributions of the eagle shape microstrip antenna array with EBG at frequencies. (a) 2.161 GHz, and (b) 9.433 GHz.

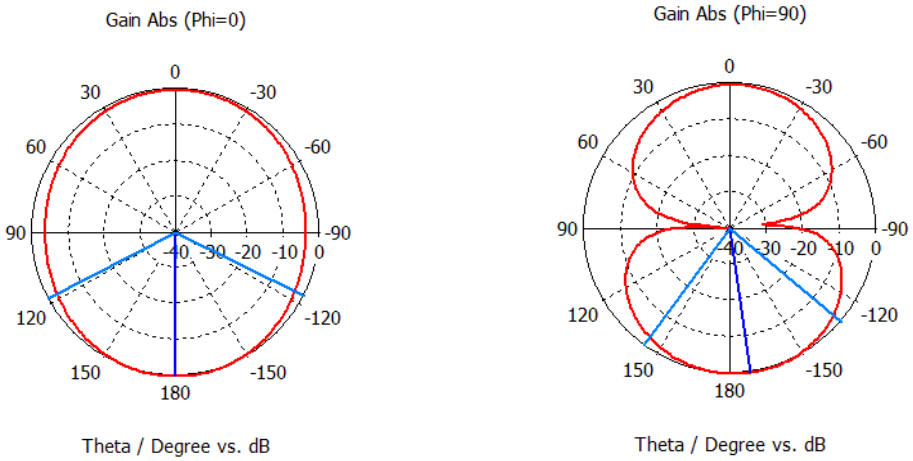

(a) (b)

Figure 17. Radiation pattern of novel eagle shape microstrip antenna array with EBG at frequency 2.161 GHz. (a) E-plane (XZ), and (b) H-plane (YZ).

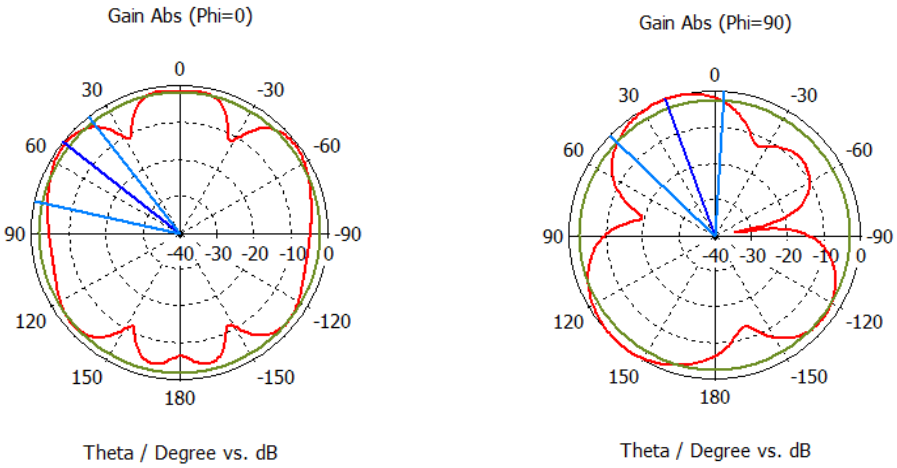

(a) (b)

Figure 18. Radiation pattern of novel eagle shape microstrip antenna array with EBG at frequency 9.433 GHz. (a) E-plane (XZ), and (b) H-plane YZ).

of the eagle wings at resonant frequency 9.433 GHz as shown in Fig. 16(b). All cells block low surface waves because the radiation is away from the wings. The E- and H-plane radiation patterns for two elements with EBG are shown in Fig. 17 and Fig. 18, respectively. The simulated gain and radiation efficiency are improved compared with without EBG case by 0.89 dBi at the first band and 1.278 dBi at the second band. The 3-dB beamwidth becomes more directive rather than single patch or array without EBG.

3. EXPERIMENTAL RESULTS AND DISCUSSION

To verify the conclusions drawn from the simulation, two microstrip antennas were fabricated on Roger RT/Duroid 5880 substrates by proto laser machine with precision 25 µm. The permittivity of the substrate is 2.2, the substrate thickness 1.5748 mm (62 mil), and tan $\delta = 0.001$. The measured results were obtained using Anritsu 37297D VNA and agree well with the simulated ones. From this experimental demonstration, it can be concluded that the EBG can be utilized to reduce the antenna mutual coupling between array elements.

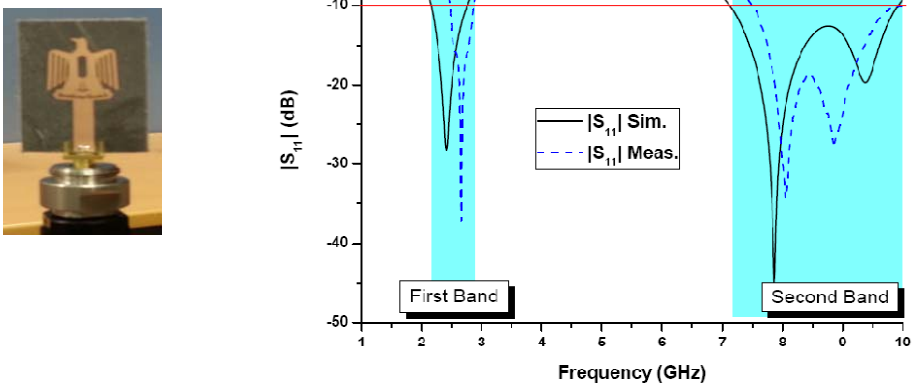

(a) (b)

Figure 19. (a) The fabricated novel eagle shape microstrip patch antenna, and (b) comparison between measured and simulated return losses.

3.1. Single Element

Figure 19(a) shows a photograph of the fabricated novel eagle-shaped microstrip patch antenna. Comparison between measured and simulated reflection coefficients is presented in Fig. 19(b). There is a little bit shift toward the upper frequencies due to the connector bonding and accuracy of fabrication because of the critical slit's dimension.

3.2. Two Elements Array without EBG

In Fig. 20(a), the fabricated two-element array of the novel eagle-shaped microstrip patch antenna array without EBG photograph is presented. The measured and simulated reflection coefficients and coupling coefficients of the two elements of the novel eagle-shaped microstrip antenna array without EBG are compared in Fig. 20(b). The measurement results give a good agreement and matching in the first band. The measured mutual coupling is better than simulated one, specially, in the second operating band. Also, there is a little bit shift toward the upper frequencies due to the connector bonding and fabrication tolerances because of the critical dimensions.

3.3. Two-Element Array with EBG

The fabricated two elements of the novel eagle-shaped microstrip patch antenna array with EBG photograph are shown in Fig. 21(a). The measured results of the two elements of the eagle-shaped microstrip antenna array without and with EBG are compared in Fig. 21(b). The measured results with EBG in the first band have a wider bandwidth than without EBG. The mutual coupling in the first and second bands are reduced by means of the EBG cells between the array elements. The results have an acceptable shift because of bonding of vias with the EBG cells and the ground plane. Also, accuracy of fabrication because of the critical slit's dimension in eagle patch and the EBG cells is the main factor in any result diffraction.

4. SAR CALCULATION

The SAR limit specified in IEEE C95.1: 2005 has been updated to 2 W/kg over any 10 g of tissue [10], which is comparable to the limit specified in the International Commission on Non-Ionizing Radiation Protection (ICNIRP) guidelines [11]. In designing antennas for wearable application, it is important to investigate the SAR value produced by the radiation from the antenna. The output power of the

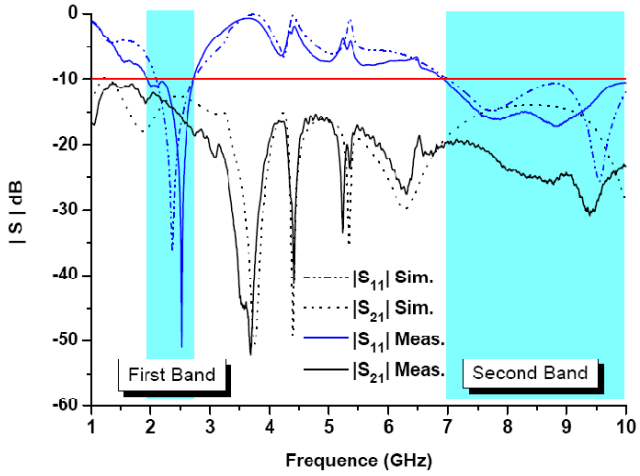

(a) (b)

Figure 20. (a) The fabricated two elements of the eagle shape microstrip patch antenna array without EBG, and (b) comparison between measured and simulated return loss and coupling coefficient.

antenna needs to be set before SAR is simulated. The reference power of the wearable antenna is set to 500 mW at the operating frequencies [12]. The SAR calculations are carried out using the CST 2014 commercial package with Hugo model CST Microwave Studio [13]; the tissues contained have relative permittivities and conductivities, according to [14, 15]. The tissues frequency dispersive properties are taken into consideration. As expected, the SAR values depend on the operating frequency, antenna type and distance between the antenna and the human body. It is noticed that the antenna fulfills the IEEE C95.1: 2005 and ICNIRP standards. In the last years, different methods to reduce the SAR produced by wearable antenna were used, specifically, auxiliary antenna elements, ferrite loading, EBG/Artificial magnetic conductors (AMC) surfaces and metamaterials [16–19]. The SAR value is influenced by various parameters such as antenna positions relative to the human body, radiation patterns of the antenna, radiation power, and antenna types [20]. The EBG structures reduce surface waves and prevent undesired radiation from the ground plane. On the other hand, extensive research efforts are exerted in minimizing wearable antennas in size and cost in conjunction with increasing the services provided by the antenna [21, 22].

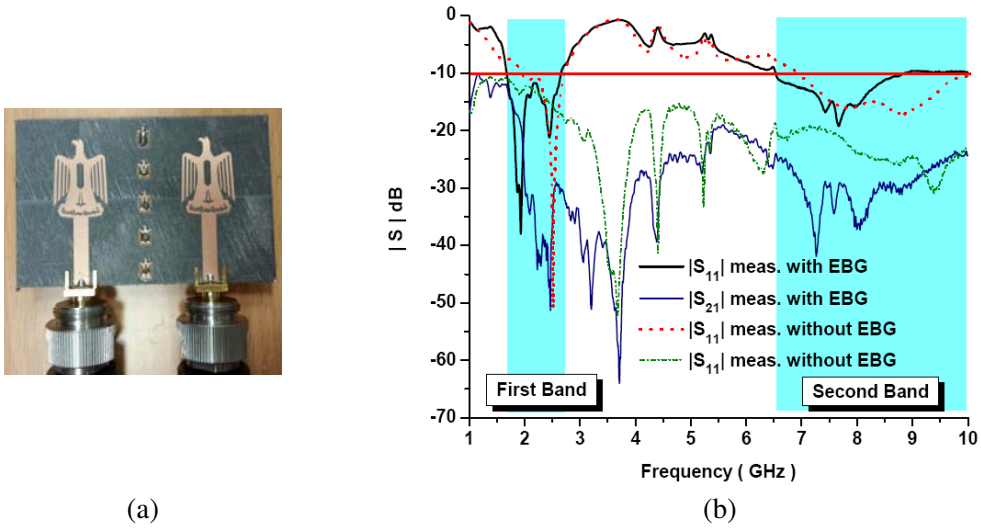

(a) (b)

Figure 21. (a) The fabricated two elements of novel eagle shape microstrip patch antenna array with EBG, and (b) comparison between measured reflection and coupling coefficients.

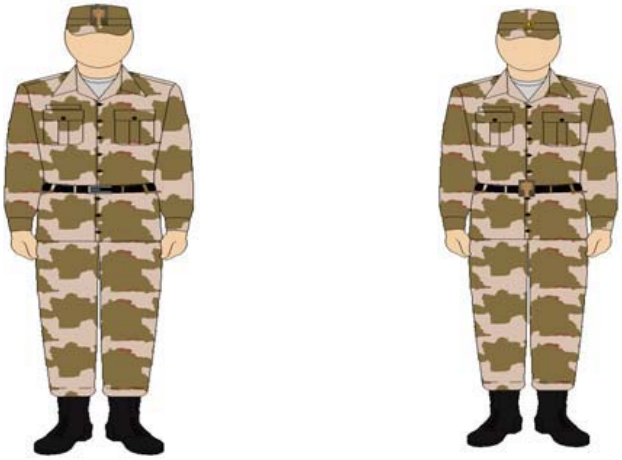

(a) (b)

Figure 22. The novel eagle shape microstrip antenna at two positions. (a) Position 1 (Head), and (b) position 2 (Belt).

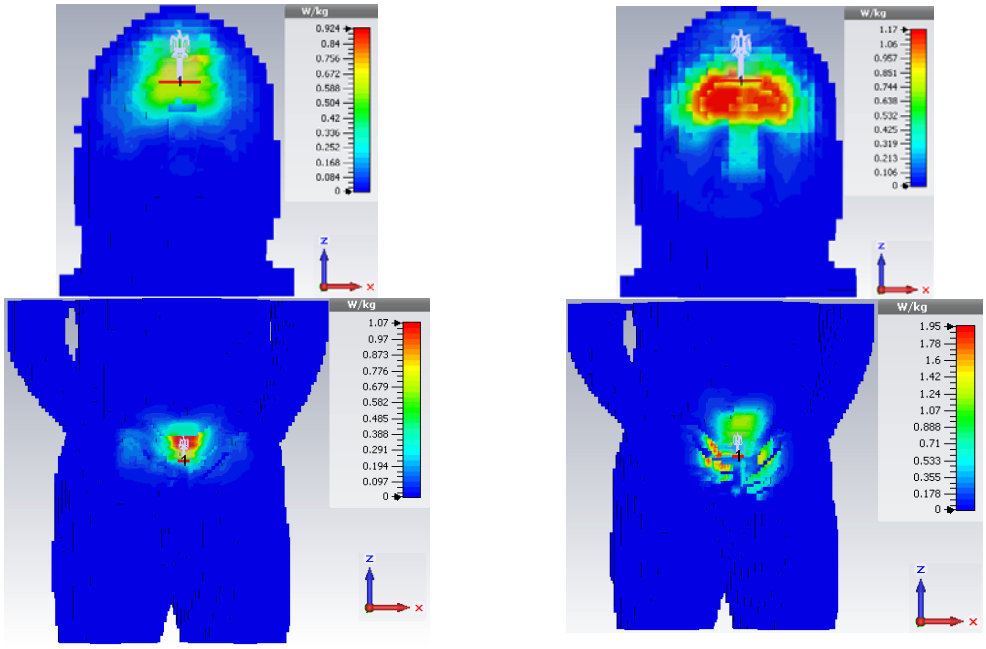

(a) (b)

Figure 23. SAR simulation for position 1 & 2 at frequencies (a) 2.42 GHz, and (b) 7.86 GHz.

Table 4. SAR of the eagle-shaped microstrip patch wearable antenna at two positions.

Frequency (GHz)	**2.42**		**7.86**	
Positions	**Position 1 (Head)**	**Position 2 (Belt)**	**Position 1 (Head)**	**Position 2 (Belt)**
SAR (w/kg) [10 g]	0.924	1.07	1.17	1.95
SAR (w/kg) [1 g]	1.514	2.27	1.82	4.28

4.1. Single Element

SAR calculation is performed at position 1 (antenna on head of the soldier) Fig. 22(a) and position 2 (antenna on belt of the soldier), Fig. 22(b). The main factor that affects the radiation on human body is the distance between the antenna and human body. The head has some important parts in human body especially the brain. So, the abdomen (belt position) is considered as an alternative place to put the antenna. The simulated SAR field distributions of the head and body phantoms in the XZ plane for the novel eagle-shaped microstrip antenna excited at 2.42 GHz and 7.86 GHz is shown in Fig. 23(a), and Fig. 23(b), respectively.

Table 4 shows the averaged 10 g and 1 g SAR at the aforementioned operating frequencies when the antenna is in close proximity to the body at the two positions (head & belt). The SAR calculations at frequency 2.4 GHz is less than that at frequency 7.86 GHz at the same positions. SAR in belt position is greater than that in head position because the voxel model has two hands beside and in front of the antenna. So, the effect of the hands increases the SAR in the abdomen region. The maximum 10 g SAR value is found to be 1.95 W/kg in the belt position at the frequency of 7.86 GHz.

4.2. Array with EBG Cells

The SAR calculations on human head model (Hugo Voxel model) in the presence of the novel eagle-shaped microstrip antenna array with EBG in the XZ plane at two frequencies (2.161 GHz, and 9.43 GHz) are shown in Fig. 24(a), and Fig. 24(b), respectively. Table 5 shows the averaged 10 g SAR at the aforementioned operating frequencies when the antenna is in close proximity to the body at

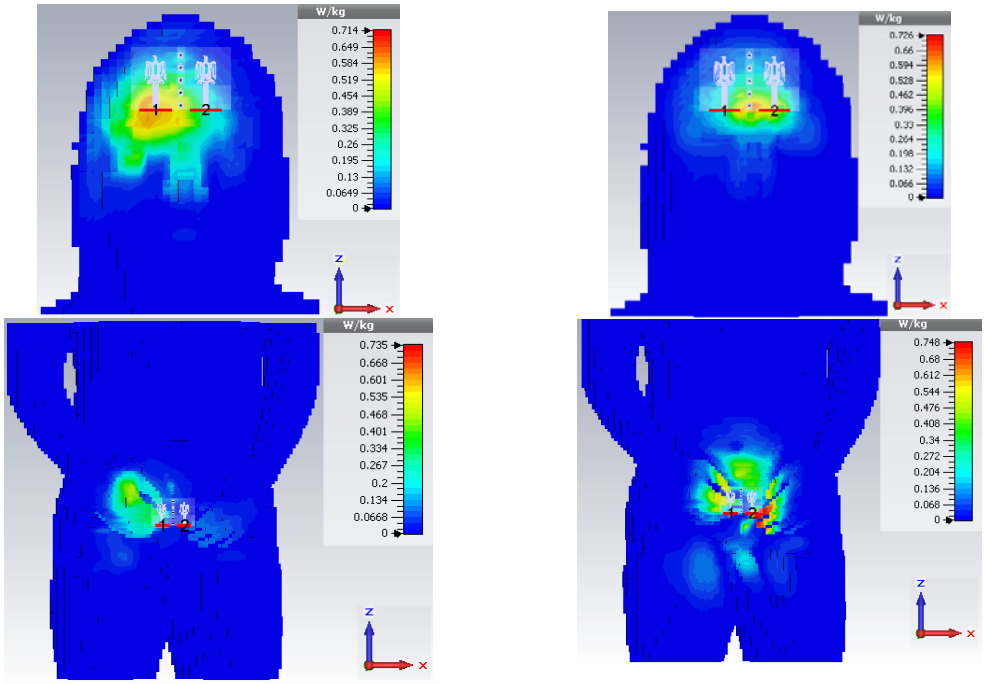

(a) (b)

Figure 24. SAR simulation for position 1 & 2 at frequencies (a) 2.161 GHz, and (b) 9.43 GHz.

Table 5. SAR of the eagle shape wearable antenna array with EBG at two positions.

Frequency (GHz)	**2.161**		**9.43**	
Positions	**Position 1 (Head)**	**Position 2 (Belt)**	**Position 1 (Head)**	**Position 2 (Belt)**
SAR (w/kg) [10 g]	0.657	0.564	0.726	0.748
SAR (w/kg) [1 g]	1.08	0.915	1.34	1.2

two positions (head & belt). The SAR calculations at frequency 2.161 GHz is less than that at frequency 9.43 GHz comparing the same positions. Because the array is more directives than single element, the SAR calculation results in array are less than in single one. Maximum SAR value of 0.748 W/kg is obtained in belt position at frequency 9.43 GHz.

5. CONCLUSIONS

In this paper, a new concept of a wearable antenna is easily integrated into clothing. A novel eagle-shaped microstrip antenna is presented. The single- and two-element antenna arrays are designed and fabricated on a substrate with dielectric constant of 2.2, thickness of 1.5748 mm, and $\tan\delta = 0.001$. The microstrip array was studied by CST simulator and fabricated by proto laser machine with precision 25 µm. The antenna can be used in official or RFID applications. This configuration is chosen because the eagle shape is the official badge for any military application. So, this antenna may be used in soldier belts, any commodity for the official application, etc. The EBG cells in the shape of small-size eagles are inserted between the adjacent coupled elements in the array to suppress the pronounced surface waves. A low mutual coupling of 36 dB is achieved at first band (1.68–2.65) GHz and 22.1 dB at second band (6.5–8.86) GHz. The measured results agree well with those obtained by the CST. SAR calculation is carried out to measure the effect of those antennas on Human bodies. Maximum SAR result is 1.953 W/kg that is acceptable to the IEEE C95.1: 2005 and the ICNIRP standards.

ACKNOWLEDGMENT

The authors acknowledge the support of Prince Sultan Advanced Technologies Research Institute (PSATRI) and KACST-TIC in Radio Frequency and Photonics (RFTONICS).

REFERENCES

1. Hall, P. S. and Y. Hao, "Antennas and propagation for body centric communications," *1st European Conference on Antennas and Propagation (EuCAP)*, Nice, Nov. 2006.
2. Hadjem, A., E. Conil, A. Gati, M. F. Wong, and J. Wiart, "Analysis of power absorbed by children's head as a result of new usages of mobile phone," *IEEE Transactions on Electromagnetic Compatibility*, Vol. 52, No. 4, 812–819, Nov. 2011.
3. Zhao, K., S. Zhang, Z. Ying, T. Bolin, and S. He, "SAR study of different MIMO antenna designs for LTE application in smart mobile handsets," *IEEE Transactions on Antennas and Propagation*, Vol. 61, No. 6, 3270–3279, Jun. 2013.
4. Parthasarathy, K. V., *Mutual Coupling in Patch Antennas*, Lap Lambert Academic Publishing, Germany, 2011.
5. Assimonis, S. D., T. V. Yioultsis, and C. S. Antonopoulos, "Design and optimization of uniplanar EBG structures for low profile antenna applications and mutual coupling reduction," *IEEE Transactions on Antennas and Propagation*, Vol. 60, No. 10, 4944–4949, Oct. 2012.
6. Exposito-Dominguez, G., J. M. Fernandez-Gonzalez, P. Padilla, and M. Sierra-Castaner, "Mutual coupling reduction using EBG in steering antennas," *IEEE Antennas and Wireless Propagation Letters*, Vol. 11, 1265–1268, 2012.
7. Hajilou, Y., H. R. Hassani, and B. Rahmati, "Mutual coupling reduction between microstrip patch antennas," *Proceedings of 6th European Conference on Antennas and Propagation (EUCAP)*, 1064–1067, Prague, Czech Republic, Mar. 2012.
8. Ahmed, M. I., E. A. Abdallah, A. A. Sebak, and H. M. ELhennawy, "Novel flagshape microstrip antenna array mutual coupling reduction," *Proceedings of 2nd Advanced Electromagnetics Symposium (AES)*, 292–298, Sharjah, United Arab Emirates, Mar. 2013.
9. Constantine, A. B., *Antenna Theory, Analysis and Design*, Chapter. 14, John Wiley & Sons, New York, 2005.
10. IEEE C95.1-2005, "IEEE standards for safety levels with respect to human exposure to radio frequency electromagnetic fields, 3 kHz to 300 GHz," Institute of Electrical and Electronics Engineers, New York, NY, 2005.
11. International Non-Ionizing Radiation Committee of the International Radiation Protection Association, "Guidelines on limits on exposure to radio frequency electromagnetic fields in the frequency range from 100 kHz to 300 GHz," *Health Physics*, Vol. 54, No. 1, 115–123, 1988.
12. Hall, P. S. and Y. Hao, *Antennas and Propagation for Body-centric Wireless Communications*, Artech House, Boston, 2012.
13. *CST Microwave Studio Suite 2014 User's Manual*, Computer Simulation Technology, Framingham, MA, USA, 2014, [Online], available:http://www.cst.com.
14. Gabriel, S., R. W. Lau, and C. Gabriel, "The dielectric properties of biological tissues. II. Measurements in the frequency range 10 Hz to 20 GHz," *Phys. Med. Biol.*, Vol. 41, 2251–2269, 1996.
15. Gabriel, C., "Tissue equivalent material for hand phantoms," *Phys. Med. Biol.*, Vol. 52, 4205–4210, 2007.
16. Ilvonen, J., O. Kivekas, J. Holopainen, R. Valkonen, K. Rasilainen, and P. Vainikainen, "Mobile terminal antenna performance with the user's hand: Effect of antenna dimensioning and location," *IEEE Antennas and Wireless Propagation Letters*, Vol. 10, 772–775, 2011.
17. Kwak, S. I., D. Sim, and J. H. Kwon, "Design of optimized multilayer PIFA with the EBG structure for SAR reduction in mobile applications," *IEEE Transactions on Electromagnetic Compatibility*, Vol. 53, No. 2, 325–333, May 2011.

18. Kwak, S. I., D. Sim, and J. H. Kwon, "SAR reduction on a mobile phone antenna using the EBG structures," *The 38th European Microwave Conference*, 1308–1311, Oct. 2008.
19. Villanueva, R. G., H. J. Aguilar, and R. L. Miranda, "State of the art methods for low SAR antenna implementation," *2010 Proceedings of the Fourth European Conference on Antennas and Propagation (EuCAP)*, 1–4, 2010.
20. Jung, M. and B. Lee, "SAR reduction for mobile phones based on analysis of EM absorbing material characteristics," *Proc. Antennas and Propagation Society International Symposium*, Vol. 2, 1017–1020, Jun. 2003.
21. Tang, C. L., J. Y. Sze, and Y. F. Wu, "A compact coupled-fed penta-band antenna for mobile phone application," *APMC*, 2260–2263, 2010.
22. Young, C. W., Y. B. Jung, and C. W. Jung, "Octaband internal antenna for 4G mobile handset," *IEEE Antennas and Wireless Propagation Letters*, Vol. 10, 817–819, 2011.